Remote Sensing of Environment 117 (2012) 366–380

Contents lists available at SciVerse ScienceDirect

Remote Sensing of Environment

journal homepage: www.elsevier.com/locate/rse

Capabilities and limitations of Landsat and land cover data for aboveground woody biomass estimation of Uganda

Valerio Avitabile [a,*], Alessandro Baccini [b], Mark A. Friedl [c], Christiane Schmullius [a]

[a] Institute of Geography, Friedrich-Schiller-University, Grietgasse 6, 07743 Jena, Germany
[b] The Woods Hole Research Center, 149 Woods Hole Road, Falmouth, MA 02540, USA
[c] Department of Geography and Environment, Boston University, 675 Commonwealth Avenue, Boston, MA 02215, USA

ARTICLE INFO

Article history:
Received 4 December 2010
Received in revised form 5 October 2011
Accepted 8 October 2011
Available online 10 November 2011

Keywords:
Biomass
Carbon
Landsat
Uganda
Forest
Land cover
LiDAR
GLAS
Regression tree
Random forest
REDD+

ABSTRACT

Aboveground woody biomass for circa-2000 is mapped at national scale in Uganda at 30-m spatial resolution on the basis of Landsat ETM+ images, a National land cover dataset and field data using an object-oriented approach. A regression tree-based model (Random Forest) produces good results (cross-validated R^2 0.81, RMSE 13 T/ha) when trained with a sufficient number of field plots representative of the vegetation variability at national scale. The Random Forest model captures non-linear relationships between satellite data and biomass density, and is able to use categorical data (land cover) in the regression to improve the results. Biomass estimates were strongly correlated ($r = 0.90$ and $r = 0.83$) with independent LiDAR measurements. In this study, we demonstrate that in certain contexts Landsat data provide the capability to spatialize field biomass measurements and produce accurate and detailed estimates of biomass distribution at national scale. We also investigate limitations of this approach, which tend to provide conservative biomass estimates. Specific limitations are mainly related to saturation of the optical signal at high biomass density and cloud cover, which hinders the compilation of a radiometrically consistent multi-temporal dataset. As a result, a Landsat mosaic created for Uganda with images acquired in the dry season during 1999–2003 does not contain phenological information useful for discriminating some vegetation types, such as deciduous formations. The addition of land cover data increases the model performance because it provides information on vegetation phenology. We note that Landsat data present higher spatial and thematic resolution compared to land cover and allow detailed and spatially continuous biomass estimates to be mapped. Fusion of satellite and ancillary data may improve biomass predictions but, to avoid error propagation, accurate, detailed and up-to-date land cover or other ancillary data are necessary.

1. Introduction

Tropical forests are attracting increasing attention within the climate change debate because of their crucial role as carbon sinks (Stephens et al., 2007) and the large emissions associated with their disappearance (Houghton, 2007; Le Quéré et al., 2009). In Africa, deforestation and forest degradation are an especially large source of greenhouse gas emissions (Bombelli et al., 2009; Canadell, Raupach, & Houghton, 2009; Houghton & Hackler, 2006).

To address this, a new mechanism is currently under negotiation by the United Nations Framework Convention on Climate Change (UNFCCC) to provide financial incentives to tropical countries to reduce emissions from deforestation and forest degradation (REDD) below a historical reference levels (Gullison et al., 2007). The implementation of such a carbon market poses several challenges (e.g. political, economical, social) (Stickler et al., 2009), but first requires the accurate assessment of the forest carbon stocks and their dynamics at national level (UNFCCC, 2009). Spatial assessment of the amount and dynamics of woody aboveground biomass (AGB) is also crucial for national planning in many tropical countries, where local communities rely on woody vegetation as a primary source of products (e.g. timber, fodder) and energy (fuelwood). Since monitoring biomass resources is an expensive and time consuming task, few developing countries have in place efficient monitoring systems. As a result, current biomass estimates for these countries are highly variable (Gibbs, Brown, Niles, & Foley, 2007; Houghton, 2005; Houghton, Lawrence, Hackler, & Brown, 2001), and sub-Saharan Africa is one of the regions with the highest uncertainty (Houghton & Hackler, 2006).

Remote sensing provides the key source of data for updated, consistent and spatially explicit assessment of biomass and its dynamics, especially in large countries with limited accessibility (DeFries et al., 2007; GOFC-GOLD, 2009; Herold & Johns, 2007; Penman et al., 2003; UNFCCC, 2007; UNFCCC, 2008). Application of remote sensing to tropical forests is particularly challenging because of complex and variable forest structure (Lu, 2005; Nelson, Kimes, Salas, & Routhier, 2000; Steininger, 2000) and difficulties obtaining high quality remote

* Corresponding author. Tel.: +49 3641 948881; fax: +49 3641 948882.
E-mail address: vale.avi@gmail.com (V. Avitabile).

0034-4257/$ – see front matter © 2011 Elsevier Inc. All rights reserved.
doi:10.1016/j.rse.2011.10.012

sensing and corresponding ground data sets (Foody, Boyd, & Cutler, 2003). To this end, a number of approaches have been proposed to map AGB from satellite observations, relating the remotely sensed data directly (mapping biomass stock) or indirectly (mapping forest cover) to biomass density (reviewed by Boyd & Danson, 2005; Lu, 2006; Goetz et al., 2009).

Several recent studies have discussed the potential and limitations of optical sensors for direct biomass or volume estimation, demonstrating the sensitivity of visible and shortwave infrared wavelengths to vegetation density and structure, which in turn are related to AGB (Baccini, Friedl, Woodcock, & Warbington, 2004; Foody et al., 2003; Gemmell, 1995; Lu, Batistella, & Moran, 2005; Lu, Mausel, Brondizio, & Moran, 2004; Steininger, 2000).

Medium resolution data (e.g. Landsat, ASTER, SPOT) are usually employed for biomass analysis at local scales (Foody et al., 2001; Hall, Skakun, Arsenault, & Case, 2006; Labrecque, Fournier, Luther, & Piercey, 2006; Lu, 2005; Muukkonen & Heiskanen, 2005; Phua & Saito, 2003; Powell et al., 2010; Zheng, Chen, Tian, Ju, & Xia, 2007; Zheng et al., 2004) and moderate to coarse resolution data (e.g. MODIS) at regional scales (Baccini, Laporte, Goetz, Sun, & Dong, 2008; Baccini et al., 2004; Blackard et al., 2008; Saatchi, Houghton, Dos Santos Alvalá, Soares, & Yu, 2007; Zhang & Kondragunta, 2006). Some studies have integrated medium and coarse resolution data (Muukkonen & Heiskanen, 2007; Tomppo, Nilsson, Rosengren, Aalto, & Kennedy, 2002). While medium resolution data provide spatial detail compatible with the size of vegetation units and biomass field observations, compiling a temporally and radiometrically consistent cloud-free datasets over large areas is not always possible. This issue is addressed by the large swath and frequent repeat cycle of moderate resolution sensors, but the limited spatial detail misses the small-scale biomass variability, and it is often difficult to relate field data with satellite observations because of mismatch in measurement scale or resolution (Baccini, Friedl, Woodcock, & Zhu, 2007). The use of Landsat data for large-area analysis has become more practical with the opening and free distribution of its archive (Woodcock et al., 2008), which has global coverage and includes nearly 40 years of data (Goward et al., 2006; Williams, Goward, & Arvidson, 2006).

Recently, the use of LiDAR (Light Detection And Ranging) remote sensing in biomass estimation has increased (Koch, 2010). Because waveform LiDAR metrics are sensitive to vertical canopy structure and the interconnection of the latter with biomass (Drake et al., 2002; Lefsky et al., 2002), several studies have found a strong linear correlation between LiDAR data and AGB (Drake et al., 2002; Drake et al., 2003; Lefsky, Harding, Cohen, Parker, & Shugart, 1999; Nelson, Krabill, & Tonelli, 1988). So far, most of the large-scale investigations have focused on sub-boreal forests (Boudreau et al., 2008; Nelson et al., 2009; Ranson et al., 2007) and few studies have applied airborne (Asner, 2009; Drake et al., 2003) or spaceborne (Baccini et al., 2008; Lefsky et al., 2005) LiDAR data in tropical areas. Airborne sensors provide highly accurate biomass estimates (Ni-Meister et al., 2010), but the associated large data volume and high costs usually limit their application to local scales. As an alternative, the Geoscience Laser Altimeter System (GLAS) sensor on board the Ice, Cloud and Elevation satellite (ICESAT) satellite has proven to be valuable for biomass and canopy height estimation over large areas (Lefsky, 2010; Lefsky et al., 2005). Since the sampling strategy of the GLAS sensor does not allow spatially continuous representation of biomass or canopy variability, GLAS data are often integrated with imaging optical systems (Baccini et al., 2008; Goetz, Sun, Baccini, & Beck, 2010; Nelson et al., 2009).

In this study, we explore capabilities and limitations of Landsat data and ancillary information (land cover) for producing high-resolution, accurate and spatially explicit AGB estimates at national scale in the tropics, to be used in support of national planning and REDD-related activities. We also use independent LiDAR measurements acquired by the GLAS sensor to assess model results.

2. Data and methods

Uganda is selected as a case-study because of the availability of an extensive biomass field dataset collected by the National Biomass Study program (Drichi, 2003), necessary for model training and validation. Because of the availability of field data for a wide range of vegetation types (e.g. woodland, shrubland, savanna), we did not limit our analysis to forests, but included all woody formations. This is especially important in the dry and semi-dry tropics where non-forest vegetation types store substantial amounts of biomass because their low biomass density is counterbalanced by coverage over large areas. In this paper, the terms biomass and AGB refer to live woody aboveground biomass.

2.1. Study area

Uganda is located along the equator in East Africa mainly between 900 and 1500 m above sea level and presents a tropical climate with two rainy seasons in the South and one in the North. It has a total area of 241,551 km2, of which subsistence cropland is the most widespread land cover type (35%), followed by grassland (21%) and woodland (16%). Water bodies cover 15% of total area (Drichi, 2003). Vegetation is mainly represented by shrubland in the north (yearly precipitation 900 mm) and grassland, woodland and forest in the south and west (yearly precipitation 1500 mm). The country biomass stock is estimated at 468 Tg of air-dry AGB, mainly located in tropical forests (29%) and woodlands (27%) (Drichi, 2003). Areas classified as cropland and grassland also store substantial amounts of biomass (24% and 10%, respectively) because of the abundance of scattered trees (Drichi, 2003; FAO, 2003).

The high economic and population growth experienced in the last 25 years has had a dramatic impact on forestry resources, which have been reduced by agricultural expansion and growing demand for charcoal, fuelwood and timber (Drichi, 2003; FAO, 2003). Woody vegetation (plantation, forest, woodland and shrubland) decreased from 26% to 20% of total area between 1990 and 2005, causing a reduction of 26% of Uganda's total biomass stock (FAO, 2006).

Uganda is expected to experience continued rapid population and economic growth in the coming years, with associated smallholder agricultural expansion into forested areas and increasing demand for forest products that will likely accelerate deforestation (FAO, 2003; Kanabahita, 2001). With 66% of the total AGB located outside of protected areas (Drichi, 2003) and insufficient incentives to pursue sustainable forest management (Kanabahita, 2001), Uganda is therefore highly relevant to REDD policies and biomass monitoring activities.

2.2. Satellite data

We compiled a mosaic of 17 Landsat L1T ETM + images acquired in the period 1999–2003 during the dry season (December to March) when cloud coverage is at a minimum and spectral separability between trees and grass/shrub is at a maximum (Table 1, Fig. 1, Fig. 2). Landsat TM data for the period of interest were not available because of missing receiving stations for central Africa (Goward et al., 2006). Due to frequent cloud cover, it was not possible to compile a single phenologically consistent dataset for the whole country. Instead, the mosaic includes 2 phenologically consistent sets of images, hereafter referred to as image "blocks", used to develop two separate biomass models. The four images located in the South-Western part of the country form "block 2" while all the other images form "block 1" (Table 1).

We also used measurements from the GLAS instrument, a waveform sampling LiDAR sensor (Schutz et al., 2005) sensitive to vegetation structure (Lefsky et al., 1999, 2005; Sun, Ranson, Kimes, Blair, & Kovacs, 2008). The LiDAR metric Height of Median Energy (HOME) is highly correlated to AGB (Baccini et al., 2008; Drake et al., 2003) and can be used as an independent comparison with the model

Table 1
Landsat acquisition date and image block number.

Path	Row	Date	Image block
170	58	10-Jan-03	1
170	59	10-Jan-03	1
170	60	10-Jan-03	1
171	57	17-Jan-03	1
171	58	17-Jan-03	1
171	59	17-Jan-03	1
171	60	18-Feb-03	1
172	57	6-Feb-02	1
172	58	6-Feb-02	1
172	59	6-Feb-02	1
172	60	31-Dec-99	2
172	61	31-Dec-99	2
173	57	15-Jan-03	1
173	58	15-Jan-03	1
173	59	27-Mar-00	1
173	60	31-Mar-03	2
173	61	31-Mar-03	2

predictions (Baccini et al., 2008). We derived the HOME metric from more than 13,000 observations acquired by GLAS Laser 2 (L2A) over the whole country in the periods January–February and October–November 2003 (Fig. **2**), after applying a screening procedure described in Baccini et al. (2008). The LiDAR measurements were compared with the biomass estimates by aggregating the HOME values within biomass classes separated by intervals of 10 Mg ha^{-1}. The linear correlation was then computed between the mean HOME value within each class and the relative value of the biomass class.

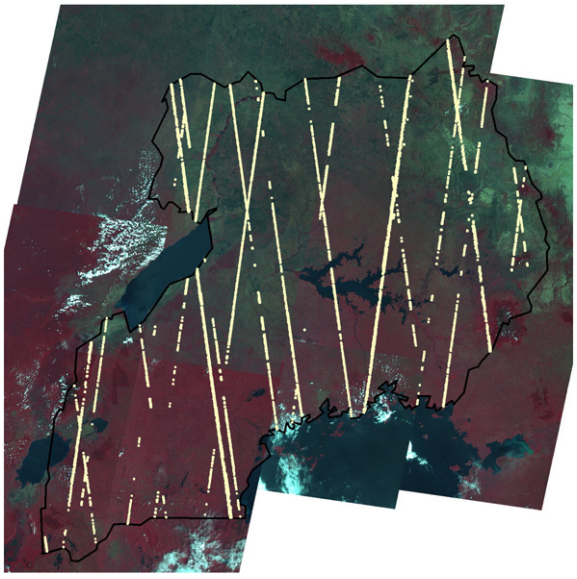

Fig. 2. Landsat mosaic (NIR, Red, Green composite) for Uganda. The yellow dots represent the selected GLAS shots.

2.2.1. Image pre-processing

2.2.1.1. Image registration. Landsat images were re-projected to a common reference system (UTM, WGS84, zone 36 N) and then co-registered. The Landsat L1T correction process utilizes both ground control points (GCP) and digital elevation models (DEM) to attain improved geodetic accuracy and a geometrically rectified product free from distortions (NASA, 2009). Therefore, image registration was a minor task, necessary only to correct for systematic shifts occurring in a few cases between neighboring images.

2.2.1.2. Radiometric correction. While accurate estimation of surface reflectance is not necessary, radiometric consistency among different images is crucial to obtain consistent results when the same regression model is applied to the images. In the absence of independent

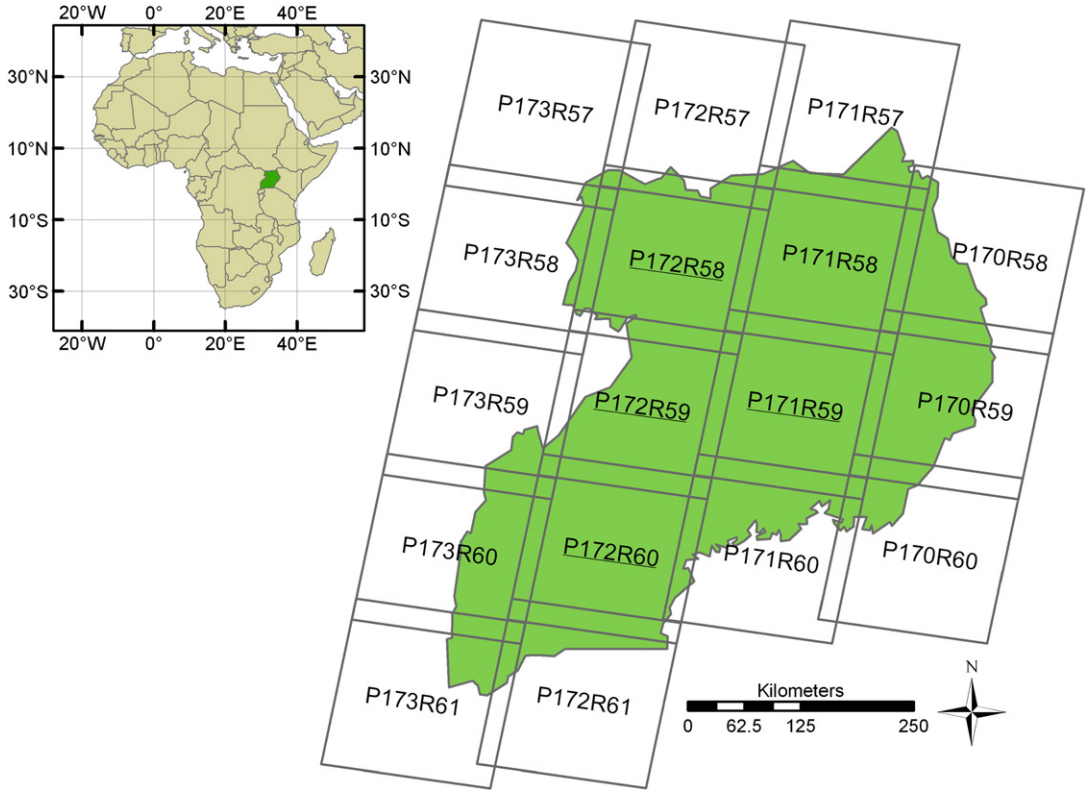

Fig. 1. Landsat Path and Row for Uganda. The underlined scenes were used as reference for the radiometric normalization of the neighboring scenes.

atmospheric data at the time and location of the image acquisition, simple absolute or relative radiometric correction methods (or their integration) are recommended over more sophisticated approaches based on atmospheric modeling (Schowengerdt, 2007; Schroeder, Cohen, Song, Canty, & Yang, 2006; Song, Woodcock, Seto, Lenney, & Macomber, 2001). The performance of an absolute and a relative correction method was first evaluated over a representative pair of neighboring Landsat images, and the correction method found to be most appropriate was applied to the complete dataset.

We performed the absolute radiometric correction using an empirical, image-based Dark Object Subtraction (DOS) approach (Chavez, 1996; Song et al., 2001). The DOS method quantifies the upwelling path radiance on the basis of dark objects present in the image, and uses constant atmospheric transmittance values. The quality of the DOS output depends on the presence of appropriate dark objects, which may not always be present in each scene. For this reason, when more than one image in the Landsat mosaic was acquired on the same date under identical atmospheric conditions, we used the darkest objects present in any of these images.

The relative radiometric calibration was performed among images located in the same image block. This procedure, also known as radiometric normalization, assumes a band-specific linear relationship between the Digital Numbers (DNs) of the same objects across time (i.e. different images). The linear equations, which are computed on the basis of radiometrically stable objects (Pseudo-Invariant Features, PIFs), transform the images to be calibrated as if they were acquired under the same atmospheric conditions and sensor characteristics of the reference image (Hall, Strebel, Nickeson, & Goetz, 1991; Schott, Salvaggio, & Volchok, 1988). We chose reference images on the basis of minimal path radiance (i.e. lower values for dark objects) and centralized position with respect to other scenes in order to minimize second-order calibration, which provides calibration of one image to a corrected image rather than to the reference image.

We evaluated the performance of the two correction approaches (absolute and relative) on the basis of changes in the Jeffrey-Matusita (JM) index (Richards, 1993) for some testing PIFs . The JM index ranges from 0 to 2 and is inversely related to the multi-dimensional spectral similarity of the objects. In order to minimize changes due to seasonal (phenology) or permanent (land cover change) effects, we selected two images acquired during the dry season separated by 7 days (Path 170 Row 58 and Path 171 Row 58). We identified 53 polygons on the overlapping area of the two images and computed the JM index for each pair of polygons before and after the radiometric correction.

2.2.1.3. Image segmentation. This analysis employed an H-resolution approach (or object-oriented approach) because the study elements in the ground scene (vegetation units uniform for biomass density class) were usually larger than the image resolution cell (30 m for Landsat) (Strahler, Woodcock, & Smith, 1986). The segmentation algorithm employed for this study is a multiple-pass region-growing method based on Euclidean distance in n-dimensional space and a minimum region size (Woodcock & Harward, 1992).

The segmentation algorithm is mainly sensitive to input bands and object size parameters. Different inputs to the segmentation algorithm were tested to identify the combination maximizing the segment's homogeneity: Landsat bands (band 3, 4, 5 and 7), Tasseled Cap components (Crist & Cicone, 1984; Kauth & Thomas, 1976) and texture channels. Texture, computed as the local minimum variance using an adaptive-window approach (Ryherd & Woodcock, 1996; Woodcock & Ryherd, 1989), was computed for Landsat bands 3, 4 and 5 with a window size ranging from 3-by-3 to 9-by-9 pixels.

The performance of the segmentation algorithm was evaluated for a test image (Path 172 Row 59) using the segment variance (σ^2_{segm}) as an indicator of the segment spectral homogeneity. Areas affected by cloud and smoke were first masked because their extreme spectral values can significantly affect the computation of the mean segment variance. Second, the average variance of all m segments was computed for each Landsat band. Then, this value was standardized (i.e. divided) by the band variance (σ^2_{band}) to compensate for different DN dynamic ranges of each band. Finally, the standardized variances were averaged through all n bands to compute the mean standardized segment variance (MSSV).

$$MSSV = \sum_{i=1}^{n} \left(\frac{\sum_{i=1}^{m} \sigma^2_{segm}}{m_{segm}} \times \frac{1}{\sigma^2_{band}} \right) \times \frac{1}{n_{band}} \quad (1)$$

The combination of inputs producing the minimum MSSV value was used to segment the Landsat mosaic.

2.2.1.4. Water and clouds mask. Water bodies, clouds and their shadows were identified and masked before the biomass analysis. For this purpose, the images were first classified at pixel level using a Maximum Likelihood classifier trained on the basis of visually-identified training areas representative of each spectral class present in the Landsat mosaic. The classified images were then thematically aggregated into 4 classes (water, clouds, shadows and everything else) and spatially aggregated at segment level using a plurality rule (i.e. selecting the most frequent class within the segment).

2.3. Field data

Uganda is one of the few African nations with a long term program aimed at the accurate assessment of biomass resources and their dynamics at country scale. The National Biomass Study (NBS) of Uganda, initiated in 1989, produced in 2003 a nation-wide biomass map based on the combination of an extensive biomass measurement field campaign and a land cover map (Drichi, 2003). Using a nation-specific data and methodology, the NBS can be considered compliant with Tier 3 of the IPCC GPG Guidelines for estimating carbon stock changes on forest lands (IPCC, 2006). Plant parameters (species, diameter at breast height (dbh), height and crown width) for all trees with dbh $\geq$ 3 cm were recorded in about 5000 plots located on a systematic grid, with sampling intensity weighted by population density (higher intensity in more densely populated areas). Plot size was 50×50 m for all land cover types except plantations, where it was 20×20 m. The Northern part of the country was under-sampled because of political instability and ongoing conflicts, while Forest Reserves were not often sampled because of difficult accessibility. Air-dry tree biomass was derived from the plant parameters using country-specific allometric equations computed on the basis of destructive sampling of 3477 trees (Drichi, 2003). The land cover map stratified the 13 main land cover types by ecological regions and biomass stock density classes, assessed through visual analysis of satellite images and field validation. The biomass map was eventually produced by applying to each land cover stratum the average biomass density of the field plots located within the unit (Drichi, 2003).

A subset of the complete field dataset was made available for this study. The subset comprised 3510 biomass plots measured between 1995 and 2005 (Fig. 3). Considering the temporal difference between the plot measurements and the image acquisition dates (up to 8 years) and possible image or plot geolocation errors, it was necessary to screen the field data to select only the plots representative of the satellite data. In particular, after visual comparison with the segmented Landsat images, we removed the plots associated with clouds or shadows, fire scars or heterogeneous image segments (i.e. segments that, due to the minimum segment size, included more than one cover type). Plots not corresponding to the images because of co-registration mismatch (e.g. low-biomass plot located inside a forest but near its edge) or land cover change such as deforestation (e.g. high-biomass plot located outside a forest but near its edge)

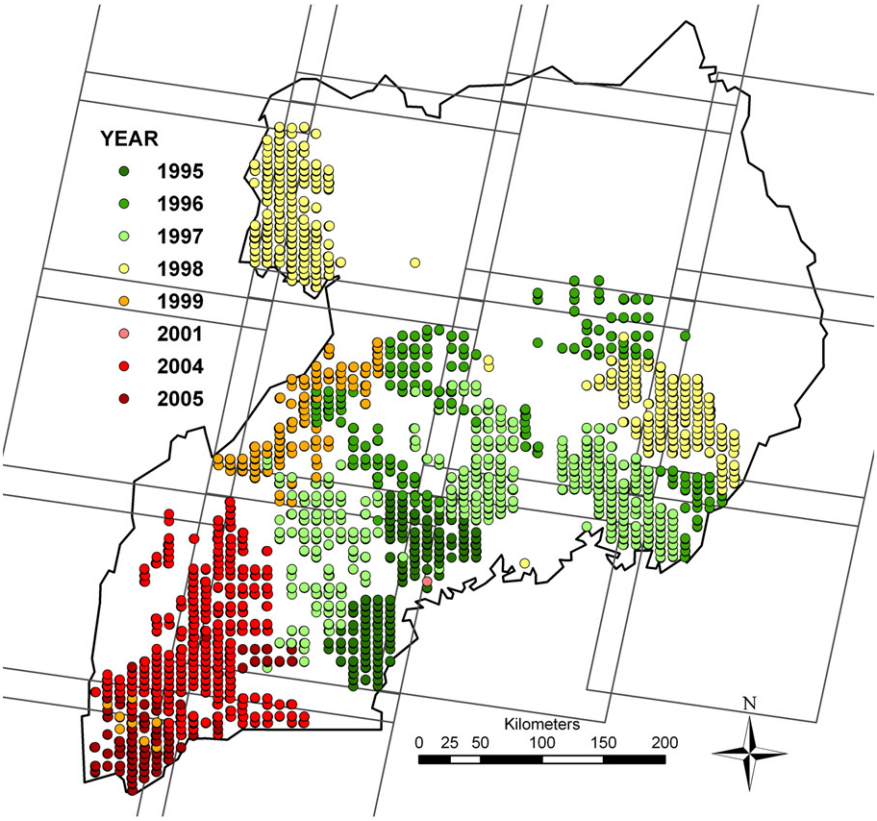

Fig. 3. Location and year of acquisition of the NBS field plots.

were also removed. However, if the mismatch between the plot and the image was due to seasonal variability of the vegetation (e.g. deciduous vegetation), the plot was retained. We note that the screening procedure did not remove errors related to field measurements and use of allometric equations, which may be relevant and propagate through the analysis (Chave et al., 2004).

2.4. Land cover data

Two land cover datasets were used for the present analysis: the Africover Multipurpose Land Cover database for Uganda (www.africover.org) and the NBS Land Cover map (Drichi, 2003). Both datasets provide a detailed land cover/use classification of Uganda for the year circa-2000, with the Africover map having higher thematic resolution and the NBS map having higher spatial resolution.

The NBS Land Cover map, given its higher spatial resolution, was used to identify the predominant land cover class of each Landsat segment, which was then used as a predictor in the biomass models. The Africover dataset, given its higher thematic detail, was used to identify the herbaceous wetlands, which were then masked in the biomass models. Masking of herbaceous wetlands was necessary because preliminary analysis showed that this vegetation type received erroneous biomass estimates by the regression models as a consequence of its spectral similarity with tropical humid forests and the absence of specific training data. We first identified the wetlands by aggregating the Africover classes with dominance of herbaceous vegetation on permanently flooded land. The biomass density of wetlands, mainly due to the presence of sparse trees, was computed as the average of the NBS biomass map within these areas and was set equal to 4 Mg ha^{-1}.

2.5. Modeling approach

Empirical, non-parametric models, such as tree-based models, neural networks, K-nearest neighbors or support vector machines, are commonly used by the remote sensing community to relate biophysical measurements with remote sensing data (Foody et al., 2003; Labrecque et al., 2006; Mäkelä & Pekkarinen, 2004; Tomppo, Gagliano, Natale, Katila, & McRoberts, 2009; Walker, Kellndorfer, LaPoint, Hoppus, & Westfall, 2007). Their strength (or weakness, from another point of view) compared to parametric models (e.g. linear regression) is that they do not assume any a-priori statistical distribution of the input data nor any specific form in the relation (e.g. linear) between the predictors and the response variable.

In the present study we used Random Forest (Breiman, 2001), an extension of tree-based models (Breiman et al., 1984) that has previously been successfully applied for biomass estimation using remote sensing data in several different contexts (Baccini et al., 2004; Baccini et al., 2008; Blackard et al., 2008; Powell et al., 2010).

The algorithm, as implemented in the open source software R (R Development Core Team, 2011), produces statistics on model performance and predictor importance (Liaw & Wiener, 2002). Model performance is computed on the basis of a cross-validation approach. For each tree the algorithm makes predictions on the data not included in the bootstrap sample, called out-of-bag (OOB) data, and aggregates these predictions to compute the overall error rate that, in the case of regression trees, is expressed as the percent of variance explained (R^2) and Root Mean Squared Error (RMSE). The OOB error rate is considered a reliable estimate of the actual model performance on independent data if the training data are not autocorrelated (De'ath & Fabricius, 2000; Liaw & Wiener, 2002). To test this assumption, we assessed the prediction accuracy on randomly selected subsets (30%, 40% and 50%) of the original dataset held out before the model development. In addition, we investigated the effect of the skewed distribution of the input data (see Section 3) on the model RMSE by randomly selecting a uniformly distributed dataset. To account for some variability in the results obtained from a random selection of original data, model performance was calculated as the average of 50 runs on different random subsets.

To evaluate the contribution of the predictor land cover to biomass estimation, we developed and compared the performance of two models for each "block" of the Landsat mosaic: the first model was based only on Landsat data (the Landsat spectral bands excluding the panchromatic and the thermal channels) and the second model was based on Landsat and land cover data. Similarly, to evaluate the advantage of using an advanced regression tree model versus more traditional approaches, the performance of Random Forest was computed and compared with that of a conventional tree-based model and a stepwise multivariate linear regression model. Finally, the image Path 172 Row 59 was used to test if additional predictors derived from Landsat (texture bands) or topographic data (altitude, slope, aspect) improved the model performance. The analyses were always performed at segment level by computing the average value of each variable within the Landsat segments and by relating this value to the average biomass density of the plots located within the training segments.

We used the percent variance explained (R^2) and the RMSE to evaluate the model performance on the complete datasets. In addition, we also computed the relative RMSE (RMSEr), the Bias and the Coefficient of Variation (CV) to assess and compare the model performance for different biomass classes. These statistics were calculated as follows, where $\hat{y}_i$ is the predicted biomass on the ith plot, y_i the observed biomass on the ith plot, $\bar{y}$ the mean biomass of n plots and $\hat{\bar{y}}$ the mean predicted biomass of n plots:

$$RMSEr = RMSE/\bar{y} \tag{2}$$

$$Bias = \hat{\bar{y}} - \bar{y} \tag{3}$$

$$CV = \sqrt{\frac{\sum_{i=1}^{n}\left(\hat{y}_i - \hat{\bar{y}}\right)^2}{n}} \times \frac{1}{\hat{\bar{y}}} \tag{4}$$

3. Results

3.1. Image pre-processing

3.1.1. Radiometric correction

We tested the performance of two correction techniques, DOS and relative calibration, using the JM distance on 53 test polygons. The average value of the JM index for all polygons was 1.70 before the correction. This parameter increased to 1.99 after the DOS correction while it decreased to 0.94 after the relative calibration (DN matching). The results suggested that the DOS reduced, instead of increasing, the spectral similarity between the two images, while the relative calibration successfully matched the images. Similar results have been observed in other studies (Schroeder et al., 2006; Song et al., 2001). The poorer performance of the DOS method may be due to the fact that the original images were already spectrally similar and the errors introduced by the DOS assumptions were larger than the atmospheric effects. As mentioned above, the DOS method is dependent on the type of dark objects present in the images and does not correct for the view path transmittance, which may be relevant for ETM bands 4, 5 and 7 (Schowengerdt, 2007). Based on these results, we performed a relative normalization of the Landsat images within each image block and used the calibrated images as input to the regression models. Specifically, the images in Path 171 and 173 were normalized to the neighboring images in Path 172, and the images in Path 170 were normalized to the neighboring images in Path 171 (Fig. 1).

3.1.2. Image segmentation

We tested several different combinations of segmentation inputs on the Landsat image Path 172 Row 59 and chose the combination producing the most spectrally homogeneous segments, according to the MSSV index. The results (Table 2) showed that the optimal combination of inputs was given by Landsat bands 3, 4, 5 and 7, while the Tasseled cap components Brightness, Greeness, Wetness (BGW) minimized the standard deviation of the segment variance. In both cases, the addition of a texture band did not reduce the MSSV.

The 17 Landsat images were segmented using bands 3, 4, 5 and 7, a maximum multi-dimensional spectral distance of 40 units, a maximum segment size for merging two adjacent regions of 500 pixels, and a minimum segment size of 20 pixels (i.e. 1.8 ha). The minimum segment size determined the Minimum Mapping Unit (MMU) of the biomass map. The mean Landsat value for each band and the predominant NBS Land Cover class (according to a plurality rule) were computed for each segment and used as inputs to the biomass models.

3.2. Field data selection

After screening the 3510 NBS field plots with the Landsat data according to the procedure presented above (Section 2.3), 27.8% of the plots were discarded because associated with clouds or shadows (1.8%), fire scars (1.3%), heterogeneous image segments (6%) or because of co-registration mismatch and land cover change (18.7%). The selected field plots (N = 2527) were then used as training data to estimate two models based on their location: Model 1 for plots located within the image block 1 and Model 2 for plots located within image block 2. The number of training data used as input to the models (N = 2734) was larger than the number of selected field plots (see Table 3) for the following reasons: a) the plots located on the overlapping area of two Landsat images acquired on different dates could have been used as training data for both images; b) when more than one plot was located within the same Landsat segment, their average biomass density was used as an input value; c) the plots with biomass density higher than 100 Mg ha^{-1} were used by both models.

The distribution of the training data (Fig. 4) was severely skewed toward smaller biomass values. The high frequency of low-biomass field plots is a direct consequence of using systematic sampling in a country dominated by croplands and grasslands. The unequal distribution of the training data affected the construction of the tree-based model, creating a larger number of nodes for low biomass values compared to those for medium and high values. Since the distribution of the training data somehow reflects the spectral variability of different biomass classes (i.e. in Uganda low-biomass areas are much more spectrally diverse than medium and high-biomass areas), the skewed distribution allowed for better estimates at low values.

Given the scarcity of field plots in dense forests, all training data with biomass higher than 100 Mg ha^{-1} were used in both models. This was necessary to provide each model with enough training data to adequately represent high-biomass classes. The use of training data derived from images that were not radiometrically calibrated was possible because of the distinct spectral signature of dense forests in comparison with that of lower biomass classes. Dense forests presented much lower spectral values in the Short Wave Infrared

Table 2
MSSV and its Standard Deviation (SD) for selected segmentation inputs on image p172r59. Inputs are coded as follow: "b" indicates Landsat bands, "Tex" indicates the Landsat band input for texture, "w" is the texture window size.

INPUTS	MSSV	SD of MSSV
b3457	0.1133	0.1316
b3457Tex3w9	0.1142	0.1360
b347	0.1157	0.1306
BGW	0.1158	0.1279
b345	0.1163	0.1346
b347Tex3	0.1283	0.1484

Table 3
Performance results on the OOB data of the Random Forest models with and without the predictor land cover (LC). Model 1 + 2 includes predictions from the two models without replicates. N is the number of input data.

	N	Landsat + LC		Landsat	
		R^2	RMSE	R^2	RMSE
Model 1	1627	0.847	13.9	0.826	14.8
Model 2	1140	0.864	15.2	0.834	16.9
Model 1 + 2	2734	0.811	12.6	0.781	13.5

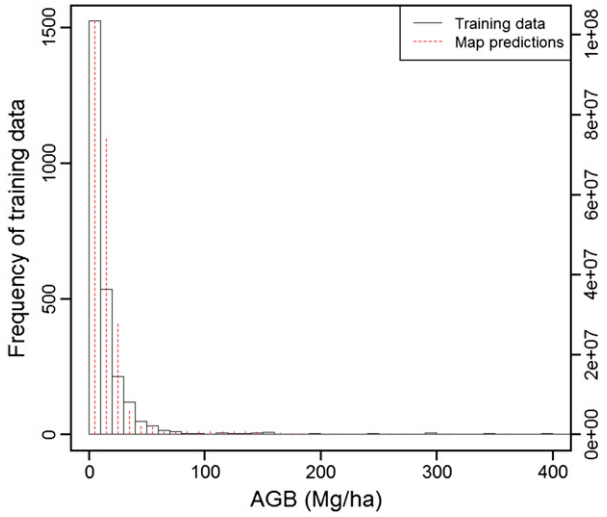

Fig. 4. Frequency distribution of the selected training data (N = 2527) and of the map predictions, in biomass bins of 10 Mg ha^{-1}. The values > 200 Mg ha^{-1} are aggregated in biomass bins of 50 Mg ha^{-1} for graphical reasons.

(SWIR) bands than other vegetation types, and small variations in their values among uncalibrated images did not affect the capability of the models to effectively separate them from other vegetation types.

3.3. Models results

We developed a biomass model (Model 1 and Model 2) for each block of the Landsat mosaic and tested their performance with and without land cover as a predictor. The results (Table 3) indicated that the four models achieved very similar results, explaining between 83% and 86% of the variance of the OOB data and presenting a RMSE between 13.9 and 16.9 Mg ha^{-1}, depending on the model and predictors. Model 2, relative to the more humid part of the country, presented slightly larger errors at low biomass values because, due to higher rainfall, spectral reflectance of low-biomass vegetation types was more variable and hence more difficult to predict. On the other hand, model predictions at high values (≥100 Mg ha^{-1}) were almost identical since the models shared the same input data.

Statistics for the complete dataset (Model 1 + 2) were computed by merging predictions from the two models without replicates (i.e. considering input data ≥ 100 Mg ha^{-1} only once) in one dataset (Table 3, Fig. 5). The performance for the complete dataset was slightly lower than that of individual models, with R^2 between 78% and 81% and RMSE between 12.6 and 13.5 Mg ha^{-1}, depending on the predictors. In all cases, the inclusion of land cover only slightly increased the overall model performance but improved biomass predictions, especially in deciduous formations where the model based only on Landsat data tended to underestimate biomass density (see Section 4). For this reason, land cover was included as a predictor variable in the biomass models.

Regarding the variable importance, which was computed as the average increase of node purity (i.e. residual sum of squares) on the OOB data that results from including each variable (Liaw, 2009), SWIR spectral bands and land cover provided the maximum contribution to the model predictions (Fig. 6) because they allowed effective separation between high and low biomass data. The important role of SWIR wavelenghts in biomass prediction is consistent with previous studies (Baccini et al., 2004; Baccini et al., 2008; Lu et al., 2004; Steininger, 2000).

The percentage variance explained by the models (R^2) was influenced by the range of the response variable, and the values reported above were positively affected by the large range of biomass values present in the training data. Considering the result from both models (Model 1 + 2), the R^2 was 0.42 for biomass values ranging from 0 to 100 Mg ha^{-1} and 0.59 for values higher than 100 Mg ha^{-1}. Model performance dropped severely for biomass values ≥ 175 Mg ha^{-1}, but this result likely reflects the small sample size (N = 16). Additional model statistics computed for each biomass class (Table 4) showed that the absolute errors (RMSE) increased for higher biomass classes, but the relative errors (RMSEr) and the normalized dispersion of the predictions (CV) decreased. While the overall bias was very small, the model tended to underestimate biomass at high values.

Considering that model residuals in our dataset tended to increase at higher biomass values, the predominance of low-biomass training

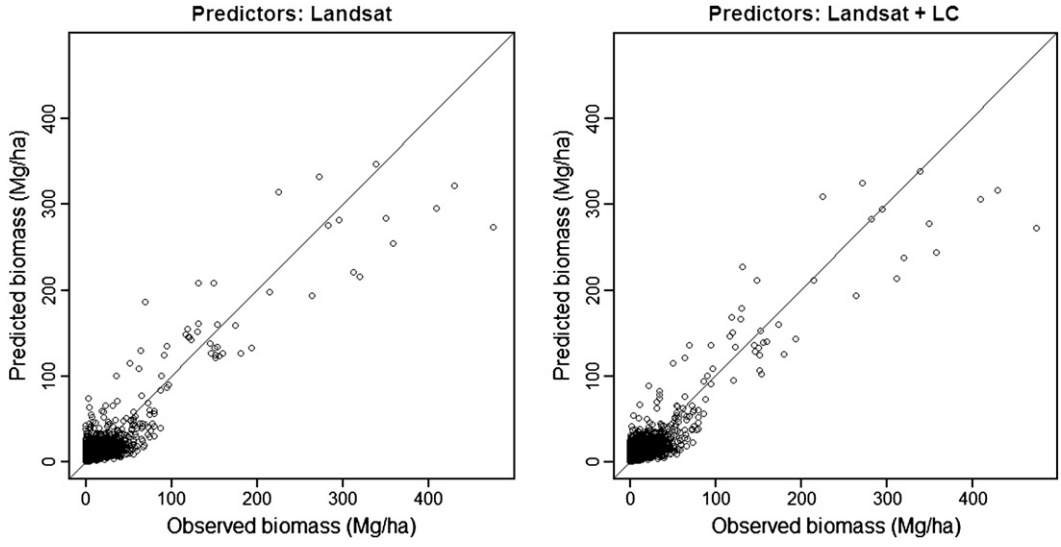

Fig. 5. Predictions of all input data (Model 1 + 2) on OOB data without (left) and with (right) the predictor land cover (LC).

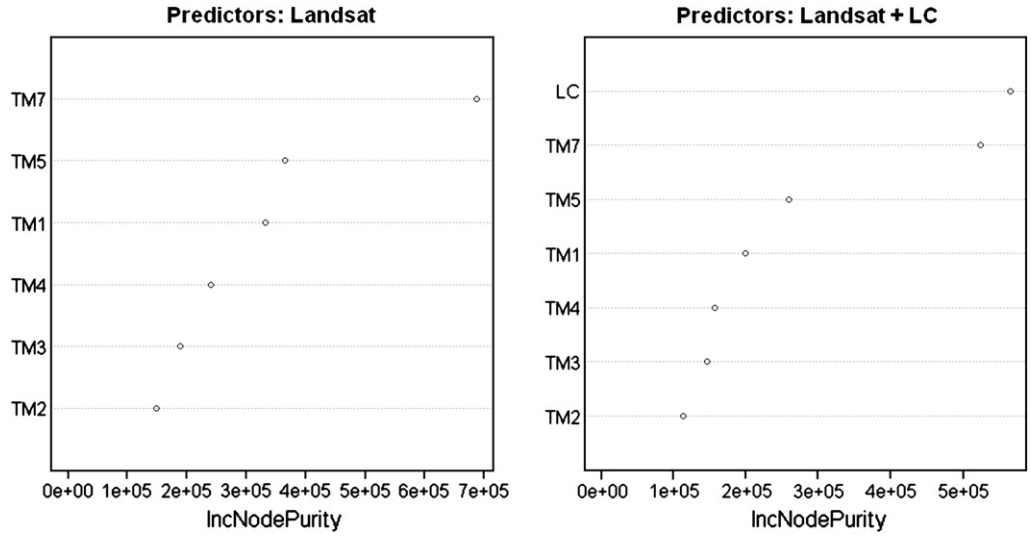

Fig. 6. Variable Importance plots for Model 1 without (left) and with (right) the predictor land cover (LC). IncNodePurity (x axis) represents the variable importance. The Variable Importance plot for Model 2 (not reported) presents the same ranking.

data biased the estimate of the model RMSE, which is clearly over-optimistic for medium and high biomass predictions. By selecting a subset of training data with uniform frequency for each biomass class (N = 44 plots), the model RMSE increased to 63.7 Mg ha^{-1} (relative RMSE 36%), which is about an average value of this parameter for the full range of values.

In order to assess the reliability of the OOB error rate estimate, the performance of Model 1 was tested against independent datasets excluded from model development by randomly selecting 30% to 50% of original data. The results (Table 5) showed that the explained variance remained above 80% and was only slightly smaller to that of the OOB data.

Random Forest also performed better than a single regression tree: the variance explained by a single tree model on the independent dataset was between 14% and 17% lower than that of Random Forest (Table 5). Another important difference between the two models is that the biomass predictions of a single regression tree are discrete, similar to those of a classification algorithm, while the predictions from Random Forest are continuous (see Fig. 7). However, due to the predominance of low biomass data in our dataset (85% of the data were below 25 Mg ha^{-1}), Random Forest did not achieve a lower RMSE than a single tree model (Table 5), showing that for very small biomass ranges the accuracy obtained with an appropriate number of discrete predictions (RPART identified 5 biomass classes smaller than 25 Mg ha^{-1}) is comparable with that of continuous estimates.

Linear models did not achieve satisfactory results when applied to our dataset. For example, a stepwise multivariate linear regression using Landsat data as predictors explained only 23% of the variance of the data in image block 1 (RMSE 31 Mg ha^{-1}, p value<0.0001). However, such poor performance was biased downward by the skewed distribution of the training data: the variance explained by the linear model increased to 65% (RMSE 71.8 Mg ha^{-1}, p value<0.0001) using training data with equal frequency for each biomass class (N = 44 plots) (Table 6), and was 40% when the model was applied to 20% of independent data randomly sampled from the uniform training dataset.

The dataset with uniform distribution for biomass class was used to compare the prediction capabilities of the three model types (Random Forest, single regression tree, stepwise multiple linear regression) using the training data, instead than on the OOB data (Table 6, Fig. 7). Since regression trees do not perform as well as linear models in predicting strongly linear relationships (De'ath & Fabricius, 2000), the lower performance of linear models supports the assumption of a complex, non-linear relationship between biomass and remotely sensed data (Baccini et al., 2004; Foody et al., 2003; Muukkonen & Heiskanen, 2005).

Finally, we tested if additional predictors derived from Landsat or topographic data improved model performance. To this end, we computed mean values for each Landsat segment of the following metrics for the test-image Path 172 Row 59: Altitude, Slope, Aspect, and Texture. Texture was derived from Landsat bands 3, 4, 5, 7 and computed as standard deviation of pixel values in a 3×3 adaptive window. The standard deviation of texture values within each segment as well as spectral values from band 6 (thermal band) were included as explanatory variables. The performance of Random Forest, computed as an average of 50 model runs, remained stable (R^2 = 0.80, RMSE = 15 Mg ha^{-1}) after the inclusion of the additional predictors. This suggests that even though some of these newly added variables are modestly important (Fig. 8), they do not contain any additional

Table 4
Performance statistics for all data (Model 1 + 2) for biomass classes in the range 0–100 Mg ha^{-1} (left column), 0–475 Mg ha^{-1} (center column) and summary statistics (right column). Due to scarcity of high biomass values, all data > 200 Mg ha^{-1} are grouped in one class.

Biomass range (Mg ha^{-1})								
	0–25	25–50	50–75	75–100	0–100	100–200	200–475	0–475
N	2388	249	50	12	2699	21	14	2734
RMSE	7.5	18.7	30.8	27.2	10.2	41.5	88.8	12.6
RMSEr	104%	55%	51%	32%	92%	29%	27%	91%
Bias	2.6	−14.0	−17.6	−11.3	0.6	1.6	−47.3	0.4
CV	67%	57%	61%	42%	91%	23%	16%	176%

Table 5
Performance of Random Forest (RF) and a single Regression Tree (RPART) for different training and testing datasets from image block 1. Predictors: Landsat bands (without LC).

		Training			Testing		Testing	
Model		RF			RF		RPART	
Dataset	N	R^2	RMSE	N	R^2	RMSE	R^2	RMSE
30% Test	1139	0.824	14.6	488	0.826	14.7	0.709	10.0
40% Test	976	0.825	15.1	651	0.812	14.5	0.683	12.4
50% Test	814	0.809	15.5	813	0.813	15.1	0.672	14.6

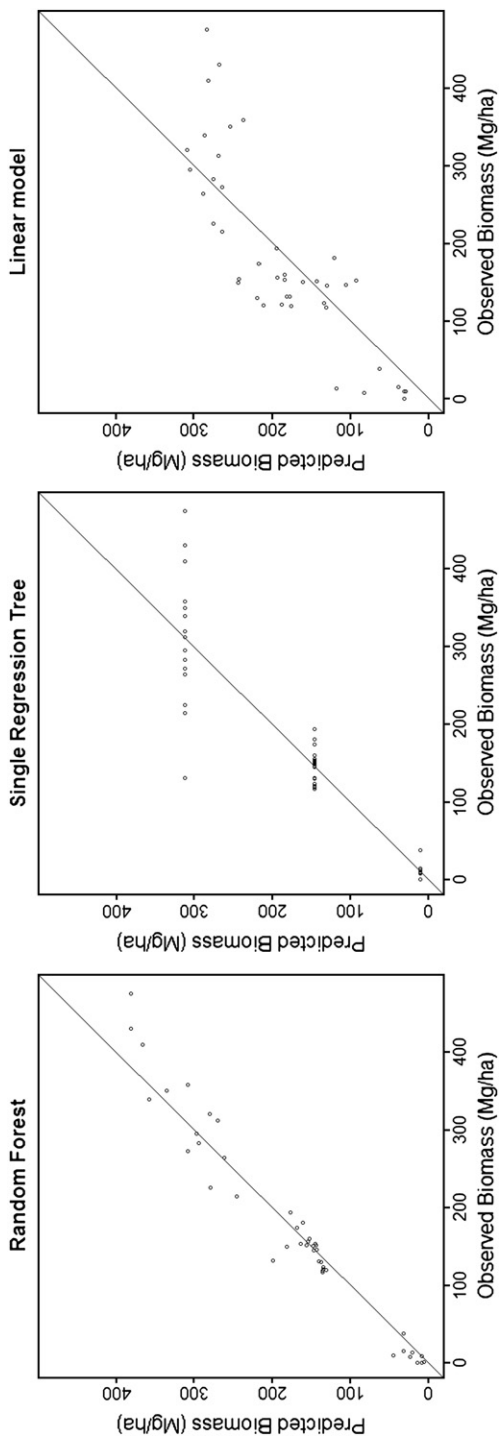

Fig. 7. Model predictions for the training data with uniform distribution per biomass class of (left to right): Random Forest, single regression tree and stepwise multiple linear regression. The black line is 1:1.

Table 6
Model performance on the training data (not on the OOB data) of the uniformly distributed dataset for Random Forest (RF), single Regression Tree (RPART), stepwise multiple linear regression (LM). Predictors: Landsat bands (without LC).

Dataset	Model	N	R^2	RMSE
Uniform distribution	RF	44	0.943	29.1
	RPART	44	0.803	53.8
	LM	44	0.651	71.8

information for biomass estimation compared to Landsat and land cover, and therefore were not employed further.

3.4. LiDAR comparison

Comparison of GLAS data with model predictions showed a strong agreement between the LiDAR HOME metric and the estimated biomass aggregated in classes of 10 Mg ha^{-1} (Fig. 9). Given the strong correlation of HOME with AGB, this result indirectly supports our biomass predictions. Correlation was higher for the model including land cover ($r = 0.90$) than for the model based only on Landsat data ($r = 0.83$), which showed a lower sensitivity to the HOME metric at intermediate biomass values (70–140 Mg ha^{-1}) In both models the standard deviation of the LiDAR metric within the biomass classes increased at higher biomass values. These results are in agreement with the model statistics (Table 3, Fig. 5), indicating that the inclusion of land cover improves prediction accuracy and that the model's accuracy decreases at higher biomass density.

3.5. Biomass map

Landsat and land cover data were used to predict AGB for each image segment using Random Forest. The biomass predictions were then mosaicked to create a map that represents the spatial distribution of live aboveground woody biomass density of Uganda for the year circa-2000 at Landsat resolution (Fig. 10). From our analysis, the aboveground biomass stock of Uganda is equal to 343 Tg. The biomass density ranges from 0 to 383 Mg ha^{-1} at the resolution of the Landsat segments; 1% of the total area (246,000 ha) is covered by clouds and shadows, and classified as "NoData". The frequency distribution of predicted biomass is similar to that of the training data (Fig. 4). The map indicates that most of the country presents low biomass density, but the contribution of these areas to the total AGB stock is important. Areas with biomass density lower than 25 Mg ha^{-1} cover about 87% of land area and store about half (53%) of total AGB stock. The remaining AGB (47%) is stored in medium and high biomass density areas covering less than 13% of land surface. Areas with medium biomass density (25–100 Mg ha^{-1}) cover about 10% of land area and store 25% of total stock, while areas with high biomass density (>100 Mg ha^{-1}) cover less than 3% of land area and store 22% of total stock. Low and medium biomass areas correspond to cropland, grassland, shrubland and woodland, while high biomass areas correspond to dense forests, mainly located within national parks and protected areas along the western border of the country.

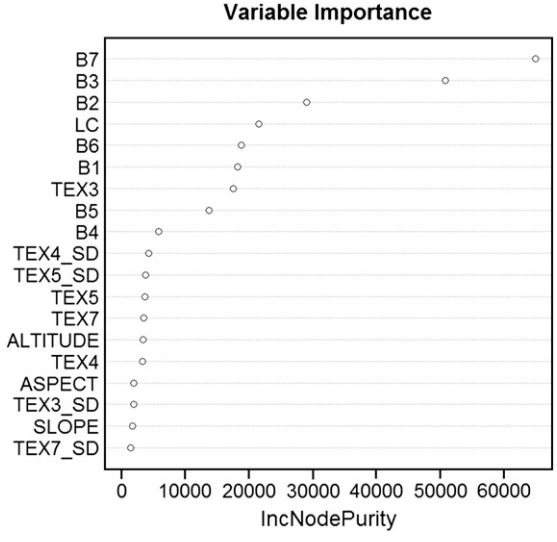

Fig. 8. Variable importance Plot for a model including the additional predictors for the image p172r59. The number after "TEX" indicates the Landsat band used to compute the Texture, the suffix "_SD" indicates the standard deviation of the texture band.

Our estimate of the total stock of Uganda is 27% lower than the NBS value (468 Mt), suggesting that our approach provides conservative biomass predictions (see Section 4). The FAO (2006) indicates that the NBS figures are relative to 1992 and reports a decrease of AGB in forests of 50 Mt (from 294 to 244 Mt) between 1992 and 2000. The NBS Report (Drichi, 2003) also indicates a decrease in biomass stock in areas outside forest during the second half of 1990's, but does not provide updated figures for the year 2000. Under the conservative assumption that biomass outside forest remained constant, the reference value of total AGB stock of Uganda for the year 2000 would be 418 Mt, reducing the difference with our estimate to 18%.

4. Discussion

The results of this study suggest that it is possible to produce spatially explicit biomass estimates at high resolution over large areas if adequate field data, satellite images and ancillary data are available. In Uganda, Landsat and land cover data were used to spatialize field biomass measurements and produce accurate (R^2 0.81) and detailed (MMU 1.8 ha) estimates at national scale that may be used for national planning or REDD-related monitoring of forest biomass. Fig. 11 shows the unprecedented spatial resolution attained with this approach in comparison with other published biomass maps.

We stress the importance of using a non-parametric regression model. Random Forest was able to capture the complex, non-linear relationship between spectral data and AGB, but required training data representative of the spectral variability within each main biomass class. Training data must be screened because the model predictions, computed as mean values within each terminal node, are sensitive to outliers. Accurate selection of the satellite data and image pre-processing are equally important to remove noise from the regression. For example, selection of images acquired during the dry season helped to avoid confusion between evergreen woody and deciduous non-woody vegetation.

Given the empirical nature of the model, it was not necessary to atmospherically correct and convert the remote sensing data to surface reflectances, but it was crucial to radiometrically calibrate the satellite images to a common scale. While we are aware that transferability over time and space of a model calibrated on a specific training dataset is limited (Foody et al., 2003), the approach, rather than the algorithm, can be easily replicated when sufficient data are available.

Landsat observations provided an effective way to spatialize field biomass measurements because the data acquired by this satellite are sensitive to vegetation structure and their spatial resolution is compatible with stand and plot size. It is well known that optical sensors are more sensitive to leaf characteristics than to the woody component of vegetation. As a result, optical data are more correlated to vegetation density than to its vertical structure, which leads to their saturation above certain biomass values. However, SWIR bands have sensitivity to canopy water content and shadow fraction, which tend to increase moving from open and monoplane to closed multilayered forest canopies (Gemmell, 1995; Steininger, 2000). If, as

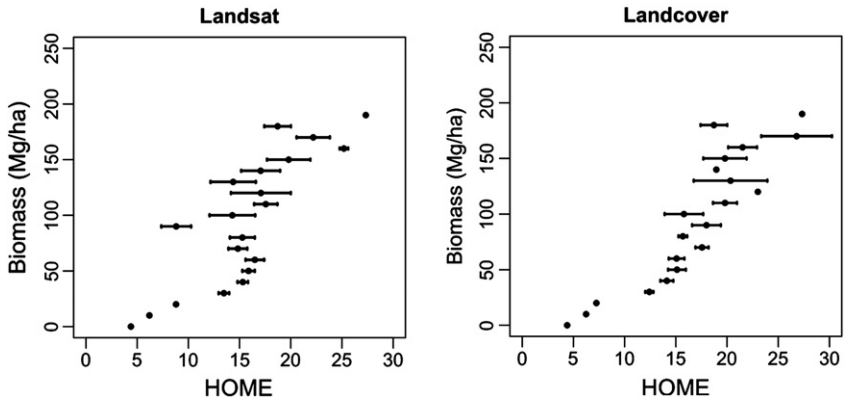

Fig. 9. Relationship between the GLAS metric HOME and predicted biomass (Mg ha^{-1}) from the model based only on Landsat (left) and including land cover (right). The horizontal bars show the standard error for the GLAS metric within biomass bin.

was the case in our study area, these canopy parameters (water content and shadow fraction) at the resolution of image segments are associated with biomass density, a non-parametric model that exploits spectral variations of SWIR bands may also have satisfactory prediction capabilities in closed canopy forests, up to a certain biomass value. In addition, image segmentation had a positive effect on the model accuracy at extreme (very high and very low) values because reducing spatial resolution also reduces the variability of the parameter to estimate. In the present study, the models tended to saturate around 150–200 Mg ha^{-1}. However, the number of high-biomass training data was too small to clearly identify the saturation threshold.

Cloud cover severely limits the amount of satellite data available in the tropics. We limited cloud coverage in the Landsat mosaic to less than 1% of land area, but cloud contamination can be expected

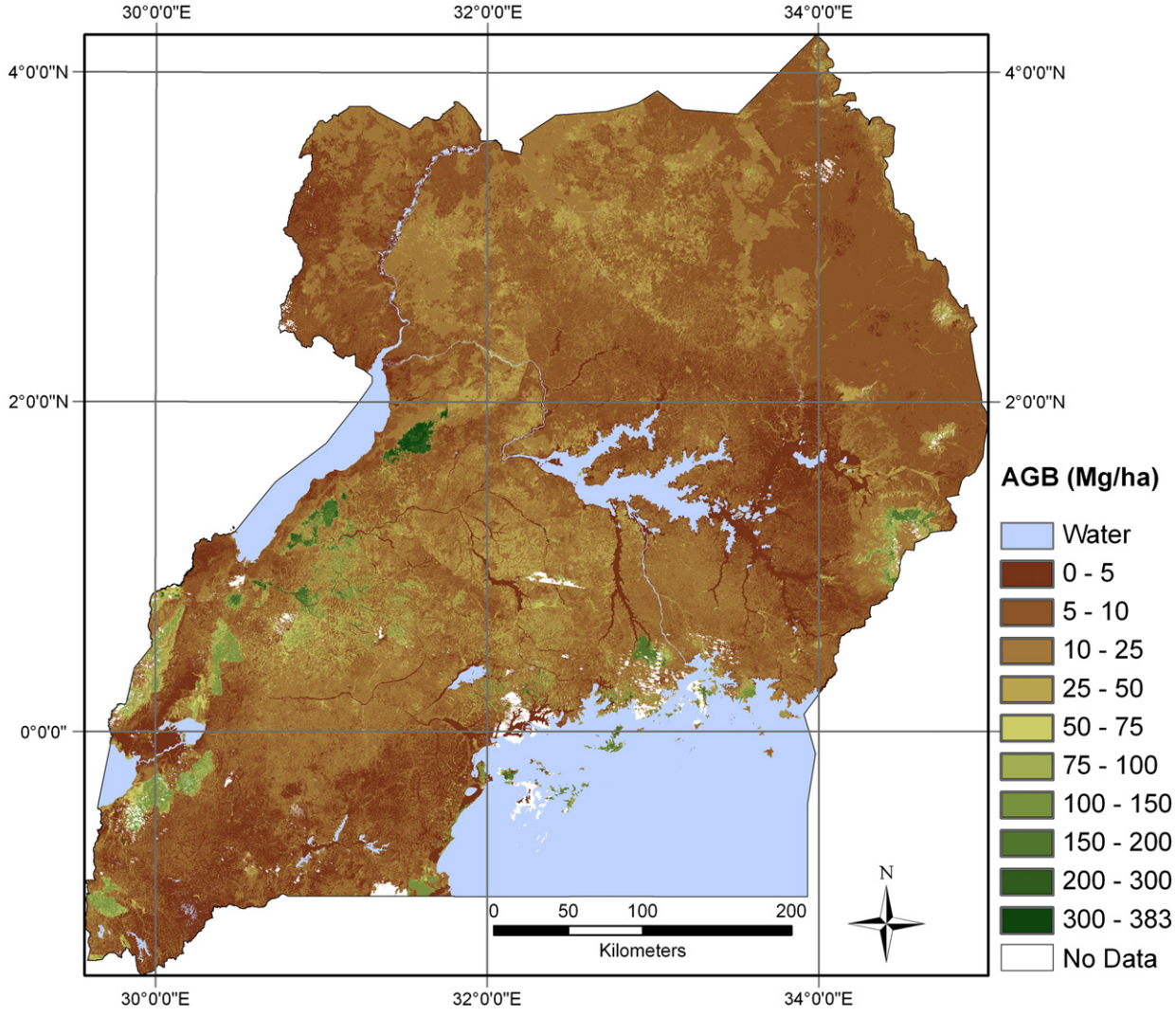

Fig. 10. AGB density map of Uganda for the year circa-2000.

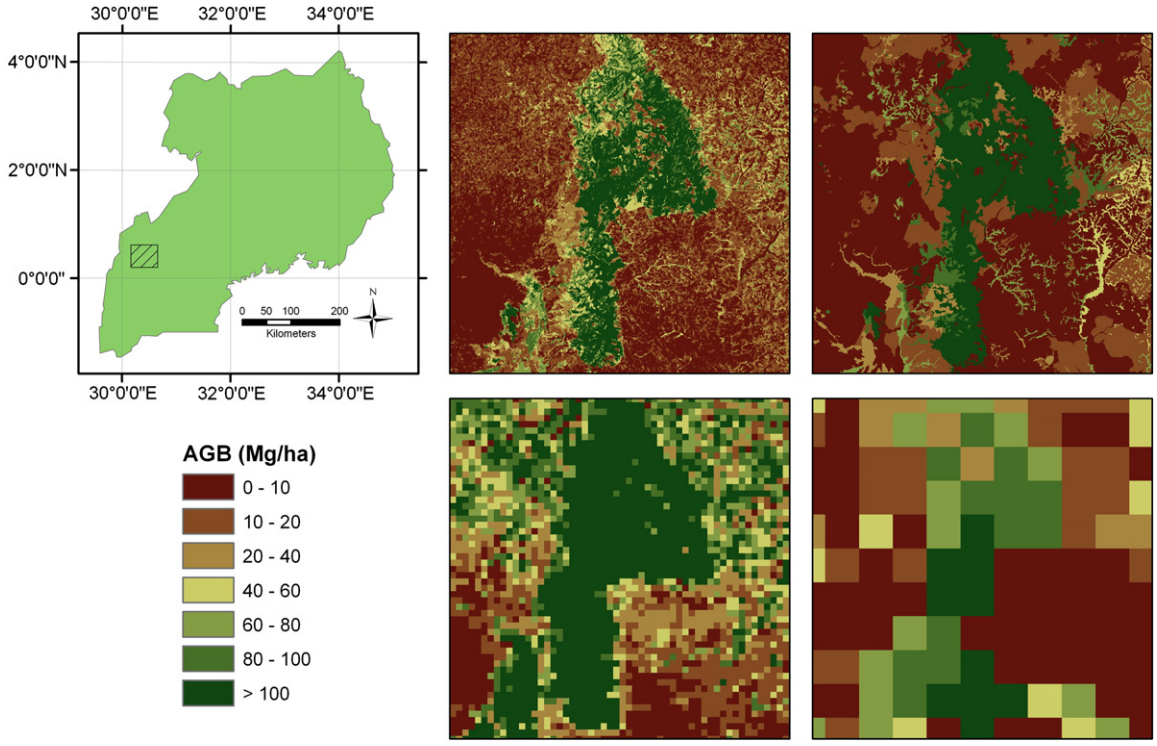

Fig. 11. Comparison of biomass maps at different resolution for a test area indicated by the black frame in the map of Uganda. The biomass maps, from up-left clockwise, are derived from Landsat and LC data at 30 m pixel resolution (this study), from national LC data (adapted from Drichi, 2003), from LC data at 5 km resolution (Gibbs & Brown, 2007) and from MODIS data at 1 km resolution (Baccini et al., 2008).

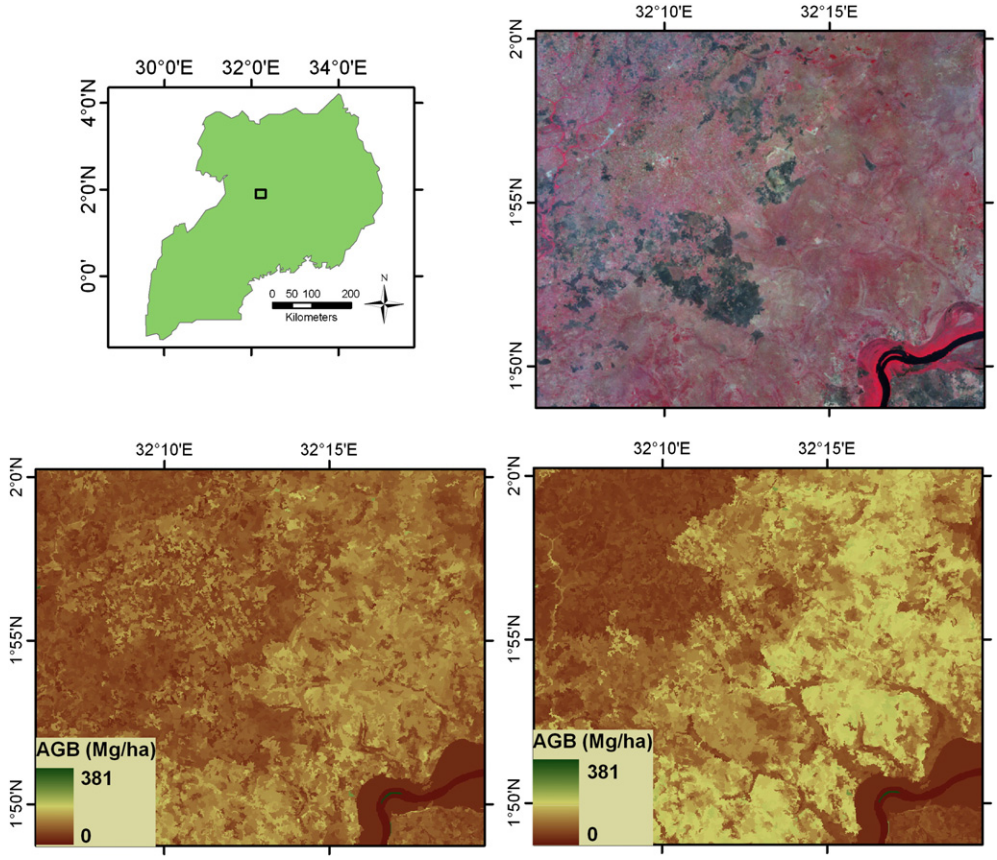

Fig. 12. Example of biomass underestimation using only Landsat data as predictor: AGB of the woodlands (10–20 Mg ha^{-1}) located in the east and south part of the Landsat image (upper-right) was underestimated by the model not including LC (lower-left), while the higher estimates (30 − 40 Mg ha^{-1}) provided by the model including LC (lower-right) were in agreement with the field data.

to be a bigger issue for larger tropical regions located in areas with persistent cloud cover (e.g. Congo basin, SE Asia). More importantly, the Landsat mosaic created for Uganda did not contain multi-temporal information because cloud coverage hindered the compilation of a consistent multi-temporal dataset, which may be important for discriminating some vegetation types (e.g. seasonal or deciduous formations). It is likely that the use of land cover as a predictor increased the model performance because it provided information related to vegetation phenology missing in the Landsat mosaic. For example, the biomass map derived only from Landsat data (acquired in the dry season) tended to underestimate the biomass content of dry deciduous shrubland and woodland compared to the NBS values, while the inclusion of land cover provided more accurate estimates for these formations (Fig. 12). On the other hand, errors and limitations of land cover data were propagated in the biomass map. For example, since deforestation in Uganda is mainly driven by small-scale local activities, it affects areas that are often smaller than the minimum mapping unit of the land cover map. As a result, the inclusion of land cover in the model caused biomass overestimation for small or partially deforested areas (Fig. 13).

We stress that Landsat data present higher spatial and thematic resolution compared to land cover, and allow the computation of spatially detailed and continuous biomass estimates. A biomass map based only on land cover data would assign the same average value to all spatial units belonging to the same class, reducing the map resolution and missing substantial spatial variability within land cover polygons. Using average biomass values for broad land cover classes can therefore cause serious underestimation of emissions from deforestation when it occurs in forests with higher than average biomass density (Houghton, 2005; Houghton & Hackler, 2006). Conversely, using average biomass values derived from traditional forest inventories may overestimate the total country stock because field data are mainly collected in the most productive forests and do not represent the overall class variability.

The analysis with LiDAR data, being an independent variable strongly related to AGB, supported the validity of this study and biomass map. The comparison indicated an overall strong linear correlation between biomass estimates and the LiDAR metric, but also lower agreement at high biomass values, especially for the model that did not include land cover data. Considering the fact that model performance decreased when applied to a smaller biomass range (Table 4) and that predictions from tree-based models tended to underestimate biomass at high values and overestimate at low values, the accuracy of biomass estimates at local scales may be lower than the overall model statistics suggest. In particular, saturation of the optical signal in closed canopy forests, model under-prediction of high biomass values, acquisition of images during the dry season and missing predictions for areas affected by cloud coverage were the main factors that tended to reduce the accuracy of our predictions and were responsible for the lower estimates of total biomass stock compared to the NBS values. Even if in some cases estimates based only on land cover data were overly optimistic for the reasons mentioned above and the true values cannot be known, our estimates were likely conservative because factors that may bias our predictions downward are predominant compared to those that may bias our predictions upward.

5. Conclusion

Accurate, updated and detailed maps of AGB distribution in tropical countries are urgently required for many different applications (e.g. REDD, global C modeling, national planning). Remote sensing data can provide an effective way to spatialize field biomass measurements. Our results show that it is possible to use freely available

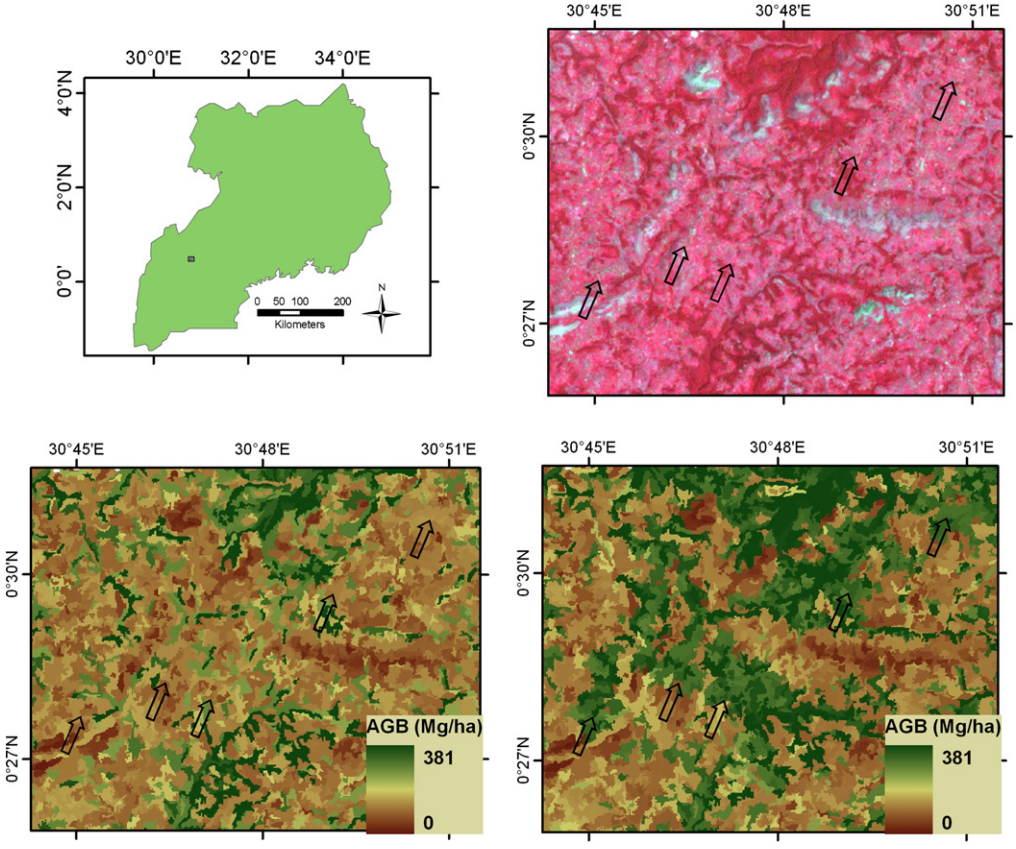

Fig. 13. Example of biomass overestimation using LC as predictor: some deforested areas indicated by arrows in the Landsat image (upper-right) are classified as forest in the LC map, increasing the biomass estimates in the model including LC (lower-right) compared to the estimates based only on Landsat data (lower-left).

optical data at 30-m resolution (Landsat) in association with a non-parametric regression tree model to estimate AGB at national level with good accuracy at high spatial resolution. This approach is particularly suited for countries with limited accessibility in dry and semi-dry areas with vegetation biomass density below the saturation threshold of optical sensors and limited cloud cover during the dry season. Integration of satellite data with land cover data improves model results but in certain cases can also negatively affect the predictions. Hence, the use of land cover or other ancillary data are recommended only when their accuracy, spatial detail and temporal resolution are comparable with those of remote sensing data. Given the sensitivity of LiDAR data to vegetation vertical structure and the strong correlation between LiDAR metrics and AGB, GLAS data may provide an effective way to complement observations from optical sensors and can be used for an independent validation of their estimates.

Acknowledgments

This work was funded by the European Commission under the Sixth Framework Programme, contract number GOCE-037132. The authors thank the Uganda National Forest Authority and the Consultative Group on International Agricultural Research (CGIAR) for data access, the Istituto Agronomico per l'Oltremare (Firenze, Italy) for administrative support, and Benjamin Devries for proof reading the final manuscript.

References

Asner, G. P. (2009). Tropical forest carbon assessment: Integrating satellite and airborne mapping approaches. *Environmental Research Letters*, *4*, 034009.

Baccini, A., Friedl, M. A., Woodcock, C. E., & Warbington, R. (2004). Forest biomass estimation over regional scales using multisource data. *Geophysical Research Letters*, *31*, 1–4.

Baccini, A., Friedl, M. A., Woodcock, C. E., & Zhu, Z. (2007). Scaling field data to calibrate and validate moderate spatial resolution remote sensing models. *Photogrammetric Engineering and Remote Sensing*, *73*(8), 945–954.

Baccini, A., Laporte, N. T., Goetz, S. J., Sun, M., & Dong, H. (2008). A first map of tropical Africa' s above-ground biomass derived from satellite imagery. *Environmental Research Letters*, *3*, 1–9.

Blackard, J. A., Finco, M. V., Helmer, E. H., Holden, G. R., Hoppus, M. L., Jacobs, D. M., et al. (2008). Mapping U.S. forest biomass using nationwide forest inventory data and moderate resolution information. *Remote Sensing of Environment*, *112*, 1658–1677.

Bombelli, A., Henry, M., Castaldi, S., Adu-Bredu, S., Arneth, A., Grandcourt, A., et al. (2009). An outlook on the Sub-Saharan Africa carbon balance. *Biogeosciences*, *6*, 2193–2205.

Boudreau, J., Nelson, R., Margolis, H., Beaudoin, A., Guindon, L., & Kimes, D. (2008). Regional aboveground forest biomass using airborne and spaceborne LiDAR in Québec. *Remote Sensing of Environment*, *112*, 3876–3890.

Boyd, D. S., & Danson, F. M. (2005). Satellite remote sensing of forest resources: Three decades of research development. *Progress in Physical Geography*, *29*(1), 1–26.

Breiman, L., Friedman, J. H., Olshen, R. A., & Stone, C. J. (1984). *Classification and regression trees.* Monterey, CA: Wadsworth and Brooks/Cole.

Breiman, L. (2001). Random forests. *Machine Learning*, *45*, 5–23.

Canadell, J. G., Raupach, M. R., & Houghton, R. A. (2009). Anthropogenic CO2 emissions in Africa. *Biogeosciences*, *6*, 463–468.

Chave, J., Condit, R., Aguilar, S., Hernandez, A., Lao, S., Perez, R., et al. (2004). Error propagation and scaling for tropical forest biomass estimates. *Philosophical Transactions of the Royal Society*, *359*(1443), 409–420.

Chavez, P. S., Jr. (1996). Image-based atmospheric corrections — Revisited and improved. *Photogrammetric Engineering & Remote Sensing*, *62*(9), 1025–1036.

Crist, E. P., & Cicone, R. C. (1984). Application of the Tasseled Cap concept to simulated thematic mapper data. *Photogrammetric Engineering and Remote Sensing*, *50*(3), 343–352.

De'ath, G., & Fabricius, K. E. (2000). Classification and regression trees: A powerful yet simple technique for ecological data analysis. *Ecology*, *81*(11), 3178–3192.

DeFries, R., Achard, F., Brown, S. L., Herold, M., Murdiyarso, D., Schlamadinger, B., et al. (2007). Earth observations for estimating greenhouse gas emissions from deforestation in developing countries. *Environmental Science & Policy*, *10*, 385–394.

Drake, J. B., Dubayah, R. O., Clark, D. B., Knox, R. G., Blair, J. B., Hofton, M. A., et al. (2002). Estimation of tropical forest structural characteristics using. *Remote Sensing of Environment*, *79*, 305–319.

Drake, J. B., Knox, R. G., Dubayah, R. O., Clark, D. B., Condit, R., Blair, J. B., et al. (2003). Above-ground biomass estimation in closed canopy Neotropical forests using lidar remote sensing factors affecting the generality of relationships. *Global Ecology and Biogeography*, *12*, 147–159.

Drichi, P. (2003). *National biomass study, technical report.* Forestry Department, Ministry of Water, Lands & Environment PO Box 1613, Kampala, Uganda.

FAO (2003). Forestry sector outlook studies for Africa. Subregional report east Africa. ftp://ftp.fao.org/docrep/fao/005/Y8693E/Y8693E00.pdf (last accessed 28/11/2010)

FAO (2006). *Global forest resources assessment 2005.* FAO forestry paper 147 Rome, Italy.

Foody, G. M., Boyd, D. S., & Cutler, M. E. (2003). Predictive relations of tropical forest biomass from Landsat TM data and their transferability between regions. *Remote Sensing of Environment*, *85*, 463–474.

Foody, G. M., Cutler, M. E., McMorrow, J., Pelz, D., Tangki, H., Boyd, D. S., et al. (2001). Mapping the biomass of Bornean tropical rain forest from remotely sensed data. *Global Ecology and Biogeography*, *10*, 379–387.

Gemmell, F. M. (1995). Effects of forest cover, terrain, and scale on timber volume estimation with Thematic Mapper data in a Rocky Mountain site. *Remote Sensing of Environment*, *51*, 291–305.

Gibbs, H. K., & Brown, S. (2007). *Geographical Distribution of Woody Biomass Carbon in Tropical Africa: An Updated Database for 2000.* Oak Ridge, Tennessee: Carbon Dioxide Information Center, Oak Ridge National Laboratory.

Gibbs, H. K., Brown, S. L., Niles, J. O., & Foley, J. A. (2007). Monitoring and estimating tropical forest carbon stocks: Making REDD a reality. *Environmental Research Letters*, *2*, 1–13.

Goetz, S. J., Baccini, A., Laporte, N. T., Johns, T., Walker, W. S., Kellndorfer, J. M., et al. (2009). Mapping and monitoring carbon stocks with satellite observations: A comparison of methods. *Carbon Balance and Management*, *4*(2), 1–7.

Goetz, S. J., Sun, M., Baccini, A., & Beck, P. S. A. (2010). Synergistic use of spaceborne lidar and optical imagery for assessing forest disturbance: An Alaska case study. *Journal of Geophysical Research*, *115*.

GOFC-GOLD (2009). *A sourcebook of methods and procedures for monitoring and reporting anthropogenic greenhouse gas emissions and removals caused by deforestation, gains and losses of carbon stocks in forest remaining forests, and forestation.* GOFC GOLD report version COP15-1, GOFC GOLD project office. Alberta, Canada: Natural Resources Canada.

Goward, S. N., Arvidson, T., Williams, D. L., Faundeen, J., Irons, J., Franks, S., et al. (2006). Historical record of Landsat global coverage: Mission operations, NSLRSDA, and International Cooperator stations. *Photogrammetric Engineering & Remote Sensing*, *72*(10), 1155–1169.

Gullison, R. E., Frumhoff, P. C., Canadell, J. G., Field, C. B., Nepstad, D. C., Hayhoe, K., et al. (2007). Tropical forests and climate policy. *Science*, *316*, 985–986.

Hall, R. J., Skakun, R. S., Arsenault, E. J., & Case, B. S. (2006). Modeling forest stand structure attributes using Landsat ETM + data: Application to mapping of aboveground biomass and stand volume. *Forest Ecology and Management*, *225*, 378–390.

Hall, F. G., Strebel, D. E., Nickeson, J. E., & Goetz, S. J. (1991). Radiometric rectification: Toward a common radiometric response among multidate, multisensor images. *Remote Sensing of Environment*, *35*, 11–27.

Herold, M., & Johns, T. (2007). Linking requirements with capabilities for deforestation monitoring in the context of the UNFCCC-REDD process. *Environmental Research Letters*, *2*, 1–7.

Houghton, R. A. (2005). Aboveground forest biomass and the global carbon balance. *Global Change Biology*, *11*, 945–958.

Houghton, R. A. (2007). Balancing the global carbon budget. *Annual Review of Earth and Planetary Sciences*, *35*, 313–347.

Houghton, R. A., & Hackler, J. L. (2006). Emissions of carbon from land use change in sub-Saharan Africa. *Journal of Geophysical Research*, *111*, G02003.

Houghton, R. A., Lawrence, K. T., Hackler, J. L., & Brown, S. (2001). The spatial distribution of forest biomass in the Brazilian Amazon: A comparison of estimates. *Global Change Biology*, *7*, 731–746.

IPCC (2006). IPCC guidelines for national greenhouse gas inventories. In H. S. Eggleston, L. Buendia, K. Miwa, T. Ngara, & K. Tanabe (Eds.), *Prepared by the National Greenhouse Gas Inventories Programme*. Japan: IGES.

Kanabahita, C. (2001). Forestry sector outlook studies. country report for Uganda. Kampala, Forestry Department, Ministry of Water, Lands & Environment. http://www.fao.org/DOCREP/004/AC427E/AC427E00.htm (last accessed 28/11/2010)

Kauth, R. J., & Thomas, G. S. (1976). The Tasselled Cap — A graphic description of the spectral–temporal development of agricultural crops as seen by Landsat. *Symposium on machine processing of remotely sensed data*. West Lafayette, IN: Purdue University 4b41–4b51.

Koch, B. (2010). Status and future of laser scanning, synthetic aperture radar and hyperspectral remote sensing data for forest biomass assessment. *ISPRS Journal of Photogrammetry and Remote Sensing*, *65*, 581–590.

Labrecque, S., Fournier, R. A., Luther, J. E., & Piercey, D. (2006). A comparison of four methods to map biomass from Landsat-TM and inventory data in western Newfoundland. *Forest Ecology and Management*, *226*, 129–144.

Le Quéré, C., Raupach, M. R., Canadell, J. G., Marland, G., Bopp, L., Ciais, P., et al. (2009). Trends in the sources and sinks of carbon dioxide. *Nature Geoscience*, *2*, 831–836.

Lefsky, M. A. (2010). A global forest canopy height map from the moderate resolution imaging spectroradiometer and the geoscience laser altimeter system. *Geophysical Research Letters*, *37*.

Lefsky, M. A., Cohen, W. B., Harding, D. J., Parker, G. G., Acker, S. A., & Gower, S. T. (2002). Lidar remote sensing of aboveground biomass in three biomes. *Global Ecology and Biogeography*, *11*, 393–399.

Lefsky, M. A., Harding, D., Cohen, W. B., Parker, G., & Shugart, H. H. (1999). Surface Lidar remote sensing of basal area and biomass in deciduous forests of eastern Maryland, USA. *Remote Sensing of Environment*, *67*, 83–98.

Lefsky, M. A., Harding, D. J., Keller, M., Cohen, W. B., Carabajal, C. C., Del Bom Espirito-Santo, F., et al. (2005). Estimates of forest canopy height and aboveground biomass using ICESat. *Geophysical Research Letters*, *32*.

Liaw, A. (2009). Package "randomForest", Breiman and Cutler's random forests for classification and regression, v.4.5-30. http://cran.r-project.org/web/packages/randomForest/randomForest.pdf (last accessed 28/11/2010)
Liaw, A., & Wiener, M. (2002). Classification and regression by random forest. *R News*, *2*(3), 18–22.
Lu, D. (2005). Aboveground biomass estimation using Landsat TM data in the Brazilian Amazon. *International Journal of Remote Sensing*, *26*(12), 2509–2525.
Lu, D. (2006). The potential and challenge of remote sensing-based biomass estimation. *International Journal of Remote Sensing*, *27*(7), 1297–1328.
Lu, D., Batistella, M., & Moran, E. (2005). Satellite estimation of aboveground biomass and impacts of forest stand structure. *Photogrammetric Engineering & Remote Sensing*, *71*(8), 967–974.
Lu, D., Mausel, P., Brondizio, E., & Moran, E. (2004). Relationships between forest stand parameters and Landsat TM spectral responses in the Brazilian Amazon Basin. *Forest Ecology and Management*, *198*, 149–167.
Mäkelä, H., & Pekkarinen, A. (2004). Estimation of forest stand volumes by Landsat TM imagery and stand-level field-inventory data. *Forest Ecology and Management*, *196*, 245–255.
Muukkonen, P., & Heiskanen, J. (2005). Estimating biomass for boreal forests using ASTER satellite data combined with standwise forest inventory data. *Remote Sensing of Environment*, *99*, 434–447.
Muukkonen, P., & Heiskanen, J. (2007). Biomass estimation over a large area based on standwise forest inventory data and ASTER and MODIS satellite data: A possibility to verify carbon inventories. *Remote Sensing of Environment*, *107*, 617–624.
NASA (2009). Landsat 7 science data users handbook. Last update August 4, 2009. http://landsathandbook.gsfc.nasa.gov/handbook/handbook_toc.html (last accessed 28/11/2010)
Nelson, R., Kimes, D. S., Salas, W. A., & Routhier, M. (2000). Secondary forest age and tropical forest biomass estimation using thematic mapper imagery. *BioScience*, *50*(5), 419–431.
Nelson, R., Krabill, W., & Tonelli, J. (1988). Estimating forest biomass and volume using airborne laser data. *Remote Sensing of Environment*, *24*, 247–267.
Nelson, R., Ranson, K., Sun, G., Kimes, D., Kharuk, V., & Montesano, P. (2009). Estimating Siberian timber volume using MODIS and ICESat/GLAS. *Remote Sensing of Environment*, *113*, 691–701.
Ni-Meister, W., Lee, S., Strahler, A. H., Woodcock, C. E., Schaaf, C., Yao, T., et al. (2010). Assessing general relationships between aboveground biomass and vegetation structure parameters for improved carbon estimate from lidar remote sensing. *Journal of Geophysical Research*, *115*.
Penman, J., Gytarsky, M., Hiraishi, T., Krug, T., Kruger, D., Pipatti, R., et al. (2003). Good practice guidance for land use, land-use change and forestry. IPCC national greenhouse gas inventories programme and institute for global environmental strategies (Kanagawa, Japan). http://www.ipcc-nggip.iges.or.jp/public/gpglulucf/gpglulucf.htm (last accessed 28/11/2010)
Phua, M. H., & Saito, H. (2003). Estimation of biomass of a mountainous tropical forest using Landsat TM data. *Canadian journal of remote sensing*, *29*(4), 429–440.
Powell, S. L., Cohen, W. B., Healey, S. P., Kennedy, R. E., Moisen, G. G., Pierce, K. B., et al. (2010). Quantification of live aboveground forest biomass dynamics with Landsat time-series and field inventory data: A comparison of empirical modeling approaches. *Remote Sensing of Environment*, *114*, 1053–1068.
R Development Core Team (2011). *R: A language and environment for statistical computing*. : R Foundation for Statistical Computing, Vienna, Austria. ISBN 3-900051-07-0.
Ranson, K. J., Nelson, R., Kimes, D., Kharuk, V., Sun, G., & Montesano, P. (2007). Using MODIS and GLAS data to develop timber volume estimates in Central Siberia. *Igarss: 2007 IEEE International Geoscience and Remote Sensing Symposium*, *1–12*, 2306–2309.
Richards, J. A. (1993). Remote sensing digital image analysis. Berlin: Springer-Verlag.
Ryherd, S., & Woodcock, C. E. (1996). Combining spectral and texture data in the segmentation of remotely sensed images. *Photogrammetric Engineering & Remote Sensing*, *62*(2), 181–194.
Saatchi, S. S., Houghton, R. A., Dos Santos Alvalá, R. C., Soares, J. V., & Yu, Y. (2007). Distribution of aboveground live biomass in the Amazon basin. *Global Change Biology*, *13*, 816–837.
Schott, J., Salvaggio, C., & Volchok, W. (1988). Radiometric scene normalization using pseudoinvariant features. *Remote Sensing of Environment*, *26*, 1–16.
Schowengerdt, R. A. (2007). *Remote sensing* Models and Methods for Image Preprocessing (Third edition). Academic Press 560 p.
Schroeder, T. A., Cohen, W. B., Song, C., Canty, M. J., & Yang, Z. (2006). Radiometric correction of multi-temporal Landsat data for characterization of early successional forest patterns in western Oregon. *Remote Sensing of Environment*, *103*, 16–26.
Schutz, B. E., Zwally, H. J., Shuman, C. A., Hancock, D., & DiMarzio, J. P. (2005). Overview of the ICESat Mission. *Geophysical Research Letters*, *32*.
Song, C., Woodcock, C. E., Seto, K. C., Lenney, M. P., & Macomber, S. A. (2001). Classification and change detection using Landsat TM data: When and how to correct atmospheric effects? *Remote Sensing of Environment*, *75*, 230–244.
Steininger, M. K. (2000). Satellite estimation of tropical secondary forest above-ground biomass: Data from Brazil and Bolivia. *International Journal of Remote Sensing*, *21*(6&7), 1139–1157.
Stephens, B. B., Gurney, K. R., Tans, P. P., Sweeney, C., Peters, W., Bruhwiler, L., et al. (2007). Weak northern and strong tropical land carbon uptake from vertical profiles of atmospheric CO2. *Science*, *316*(5832), 1732–1735.
Stickler, C. M., Nepstad, D. C., Coe, M. T., McGrath, D. G., Rodrigues, H. O., Walker, W. S., et al. (2009). The potential ecological costs and cobenefits of REDD: A critical review and case study from the Amazon region. *Global Change Biology*, *15*(12), 2803–2824.
Strahler, A. H., Woodcock, C. E., & Smith, J. A. (1986). The nature of models in remote sensing. *Remote Sensing of Environment*, *20*, 121–139.
Sun, G., Ranson, K., Kimes, D., Blair, J., & Kovacs, K. (2008). Forest vertical structure from GLAS: An evaluation using LVIS and SRTM data. *Remote Sensing of Environment*, *112*(1), 107–117.
Tomppo, E. O., Gagliano, C., Natale, F. D., Katila, M., & McRoberts, R. E. (2009). Remote sensing of environment predicting categorical forest variables using an improved k-Nearest neighbour estimator and Landsat imagery. *Remote Sensing of Environment*, *113*, 500–517.
Tomppo, E. O., Nilsson, M., Rosengren, M., Aalto, P., & Kennedy, P. (2002). Simultaneous use of Landsat-TM and IRS-1C WiFS data in estimating large area tree stem volume and aboveground biomass. *Remote Sensing of Environment*, *82*, 156–171.
UNFCCC (2007). Report on the second workshop on reducing emissions from deforestation in developing countries. http://unfccc.int/resource/docs/2007/sbsta/eng/03.pdf (last accessed 28/11/2010)
UNFCCC (2008). *Report on the workshop on methodological issues relating to reducing emissions from deforestation and forest degradation in developing countries.* FCCC/SBSTA/2008/11..
UNFCCC (2009). *Reducing emissions from deforestation in developing countries: Approaches to stimulate action.* FCCC/SBSTA/2009/19/Add.1.
Walker, W. S., Kellndorfer, J. M., LaPoint, E., Hoppus, M. L., & Westfall, J. (2007). An empirical InSAR-optical fusion approach to mapping vegetation canopy height. *Remote Sensing of Environment*, *109*, 482–499.
Williams, D. L., Goward, S. N., & Arvidson, T. (2006). Landsat: Yesterday, today, and tomorrow. *Photogrammetric Engineering & Remote Sensing*, *72*(10), 1171–1178.
Woodcock, C. E., Allen, R., Anderson, M., Belward, A., Bindschadler, R., Cohen, W., et al. (2008). Free access to Landsat imagery. *Science*, *320*(5879), 1011.
Woodcock, C. E., & Harward, V. J. (1992). Nested-hierarchical scene models and image segmentation. *International Journal of Remote Sensing*, *13*(16), 3167–3187.
Woodcock, C. E., & Ryherd, S. L. (1989). Generation of texture images using adaptive windows. *Technical Papers, ASPRS/ACSM Annual Convention*, *2*. (pp. 11–22) 2–7 April, Baltimore, Maryland.
Zhang, X., & Kondragunta, S. (2006). Estimating forest biomass in the USA using generalized allometric models and MODIS land products. *Geophysical Research Letters*, *33*(9), 1–5.
Zheng, G., Chen, J. M., Tian, Q. J., Ju, W. M., & Xia, X. Q. (2007). Combining remote sensing imagery and forest age inventory for biomass mapping. *Journal of Environmental Management*, *85*, 616–623.
Zheng, D., Rademacher, J., Chen, J., Crow, T., Bresee, M., Le Moin, J., et al. (2004). Estimating aboveground biomass using Landsat 7 ETM+ data across a managed landscape in northern Wisconsin, USA. *Remote Sensing of Environment*, *93*, 402–411.